ACS OMEGA

http://pubs.acs.org/journal/acsodf

Article

Strain Effects on the Growth of $La_{0.7}Sr_{0.3}MnO_3$ (LSMO)−NiO Nanocomposite Thin Films via Substrate Control

Bethany X. Rutherford, Bruce Zhang, Xuejing Wang, Xing Sun, Zhimin Qi, Han Wang, and Haiyan Wang*

Cite This: *ACS Omega* 2020, 5, 23793−23798

Read Online

ACCESS | Metrics & More | Article Recommendations | Supporting Information

ABSTRACT: Oxide-oxide-based vertically aligned nanocomposites (VANs) have demonstrated a new material platform for enhanced and/or combined functionalities because of their unique vertical geometry and strain coupling. Various factors contribute to the growth of VANs, including deposition parameters, phase composition, phase ratios, crystallography, etc. In this work, substrate strain effects are explored through growing a two-phase oxide-oxide $La_{0.7}Sr_{0.3}MnO_3$ (LSMO):NiO system, combining antiferromagnetic NiO and ferromagnetic LSMO, on various substrates with different lattice parameters. The X-ray diffraction (XRD), transmission electron microscopy (TEM), and magnetic property measurements all suggest that substrate strain plays a critical role in the epitaxial growth of a VAN structure and their two-phase separation, and thus results in different physical properties. This work sheds light on the fundamental nucleation and growth mechanisms of the two-phase VAN systems and the effects of substrate strain on the overall orientation and growth quality of the VAN films.

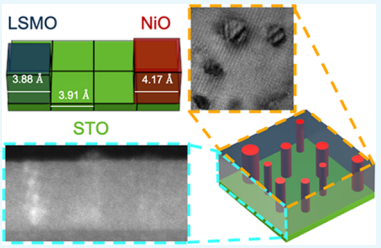

INTRODUCTION

Nanocomposite thin films combine two or more materials into one to create nanoscale features, making them more interesting as electronic devices shrink in weight and size. These nanocomposite thin films offer a multifunctional material solution to device size reduction in various applications such as personal electronics, memory and data storage devices, photonic devices, optoelectronics, and superconductors.[1−3] A major effort in the community has been improving their functionality—magnetic,[2,4,5] optical,[6] electrical properties,[7] etc. Among various nanocomposite materials, oxide−oxide-based vertically aligned nanocomposite (VAN) thin-film materials have demonstrated opportunities in achieving enhanced functionality and the potential for being multifunctional due to their unique vertical geometry and therefore strong vertical strain coupling. Oxide-oxide nanocomposite systems have demonstrated applications as superconductors,[8,9] solid oxide fuel cells (SOFCs),[10] multiferroic,[11,12] and photonic devices.[13] It has been reported that the structure and morphology of nanocomposite materials influence the overall properties, therefore tuning their overall morphology will subsequently tune their physical properties.[2,4,14−17] This has placed an emphasis on the initial nucleation and growth, ordering, and uniformity of the nanocomposite structures, i.e., creating consistent structures such as nanopillars, nanolayers, and nanoparticles across the entire material that are functional for larger-scale samples.[18,19]

The epitaxial growth of two phases in VAN structures has been reported as a critical factor for the overall film quality of the VAN systems.[15,16,19−21] To enable epitaxial growth, the small lattice mismatch between the film phases and the underlying substrate (typically $f < 7\%$) is typically preferred; for example, $La_{0.7}Sr_{0.3}MnO_3$ (LSMO):ZnO on strontium titanate (STO) substrates and $BiFeO_3$:Sm_2O_3 on STO substrates present ideal in-plane matching to the underlying substrates.[15,22−25] Other factors, such as various deposition parameters—phase selection, lattice parameters, crystallography, etc.—have been found to effectively tune the growth morphology of the VANs. For example, deposition frequency influences nanopillar width.[20,26] An in-plane strain compensation model has been theorized in VANs, where the two phases with opposite strain states relative to the underlying substrate present a more ordered two-phase distribution in-plane compared with those with perfect lattice matching conditions.[1] A recently reported study on TaN:Au VAN system grown on MgO substrates presents a highly ordered hexagonal close-packed pillar geometry, which is believed to be due in part to the in-plane strain compensation of compressive strain of TaN (a_{TaN} = 4.37 Å) on MgO (a_{MgO} = 4.21 Å) and tensile strain of Au (a_{Au} = 4.065 Å) on MgO.[27] These studies all suggest that substrate strain plays a critical role in the overall nucleation and growth of VAN systems.

Received: June 17, 2020
Accepted: August 24, 2020
Published: September 8, 2020

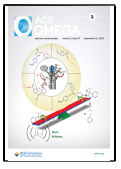

https://dx.doi.org/10.1021/acsomega.0c02923
ACS Omega 2020, 5, 23793−23798

To explore such in-plane strain effects on the overall VAN growth and the range of strain compensation model, in this work, a set of LSMO:NiO VAN films (<20 nm) were designed to investigate the substrate strain effect with limited vertical strain effect. These films have been deposited on various substrates: $SrTiO_3$ (STO), $LaAlO_3$ (LAO), and MgO (a_{MgO} = 4.21 Å, a_{STO} = 3.91 Å, and a_{LAO} = 3.79 Å). A LSMO:NiO system couples ferromagnetic LSMO with antiferromagnetic NiO in a VAN fashion, creating more interfacial area for coupling and therefore leading to interesting properties such as exchange bias coupling and enhanced magneto-transport between the two materials.[5] LSMO:NiO VAN thin films have been reported to grow epitaxially on single-crystal STO substrates, where the lattice parameters of LSMO and NiO are 3.88 and 4.17 Å, respectively, for cube-on-cube growth.[16,28] A comparison of the lattice parameters of the substrates and the two phases of the target used for deposition is shown in Figure 1 in the predicted cube-on-cube growth orientation. It is

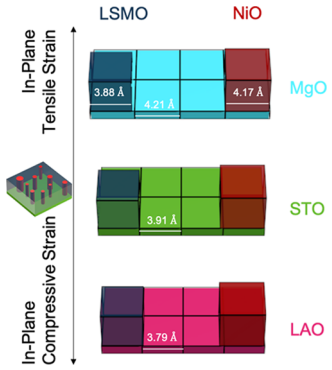

Figure 1. Lattice parameter comparison of LSMO and NiO phases on LAO, STO, and MgO substrates.

hypothesized that altering the lattice mismatch-induced strain from the different substrates could lead to different two-phase distributions based on the above-mentioned strain compensation model. Lattice mismatch-induced strain has been shown to influence other film properties such as critical film thickness as a higher mismatch percentage tends to lead to lower thicknesses.[25] Strain engineering has also been used previously to manipulate the overall nanopillar shape through altering the strain of the deposition surface.[29] As mentioned previously, film-substrate strain could also play a role in the overall two-phase nucleation and distribution of VAN structures on the substrate based on the in-plane strain compensation model.[1] It is expected that the strain could affect the overall distribution of the two phases, NiO and LSMO, and thus the exchange bias coupling between the ferromagnetic LSMO and the antiferromagnetic NiO. More specifically, different substrates placing both LSMO and NiO phases in tension or compression could cause a change in the overall nanostructure to compensate for the mismatch strain, such as alterations in the size or density of nanopillars to increase or decrease to compensate for the increased total strain state. XRD, transmission electron microscopy (TEM), and scanning transmission electron microscopy (STEM)/electron dispersive spectroscopy (EDS) are used to explore the overall two-phase morphologies based on the substrates along with conducting magnetic measurements to explore the overall ferromagnetic properties and anisotropy, coupled with the microstructural characteristics of the films.

RESULTS AND DISCUSSION

As shown in the XRD θ–2θ scans in Figure 2a, the two phases, LSMO and NiO, clearly separated on the STO (001)

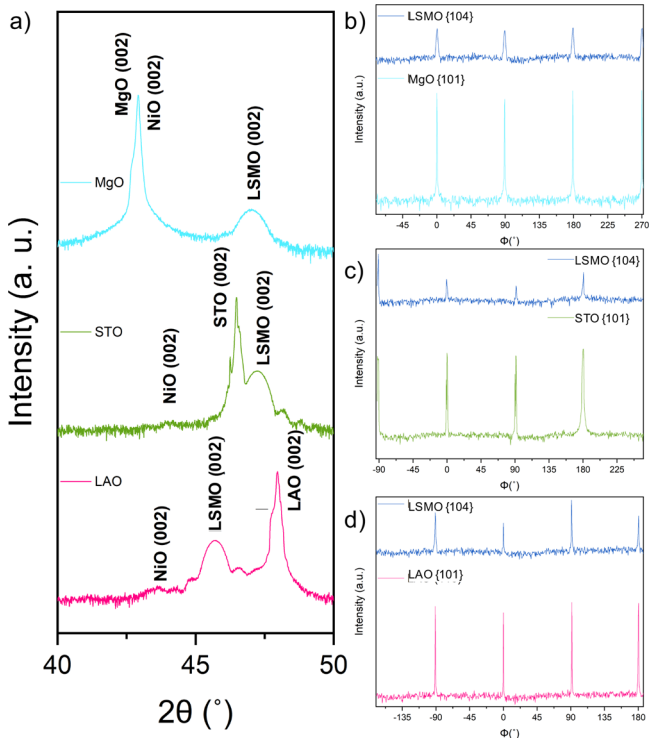

Figure 2. (a) θ–2θ XRD results for the LSMO:NiO films grown on LAO, STO, and MgO substrates under the same growth conditions and (b–d) phi-scan for LSMO on MgO, STO, and LAO, respectively.

substrate, as is seen in the LSMO and NiO (002) peaks, similar to previously reported work on this system.[5] The mismatch strain between the substrate lattice and the deposited LSMO and NiO alter the peak positions of the deposited material. This is especially noticeable in the highly strained LSMO (002) peak on the LAO substrate. Due to the potential overlapping of the film peaks with the LAO and MgO substrate peaks, LSMO and NiO phase separation is not apparent in the θ–2θ scans. In parallel, to understand the in-plane orientation relationship, a detailed XRD phi-scan was conducted as shown in Figure 2b–d for each sample. The LSMO {104} and STO {101} crystallographic planes were chosen for the phi-scan measurements. From the phi-scans of all three thin films, the LSMO shows fourfold symmetry, indicating that LSMO has grown in a cube-on-cube manner without any in-plane rotation. The lattice mismatch of the LSMO phase grown on the LAO, STO, and MgO are −2.3, −0.8, and 8.5%, respectively. For the NiO phase, the calculated lattice mismatch values on the LAO, STO, and MgO films are −9.1, −6.2, and 1.0%, respectively. These results suggest that substrate strain from the difference in lattice parameters can influence the crystallography orientation of the two phases in the nanocomposite thin-film materials and strains nearing 1% in at least one phase are high enough to cause an indistinct nanostructure to form instead of a clear two-phase structure such as a multilayer or VAN.

This phase separation was further confirmed through the TEM and EDS mapping seen in Figure 3. Figure 3a–c depicts the cross-section of the film grown on STO. The NiO pillars

https://dx.doi.org/10.1021/acsomega.0c02923
ACS Omega 2020, 5, 23793–23798

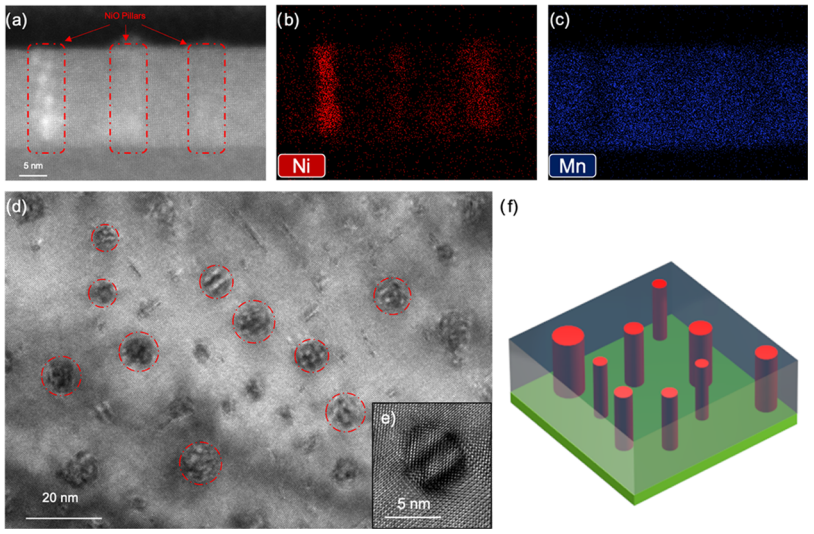

Figure 3. (a) Cross-sectional TEM image of LSMO:NiO nanocomposite thin film on STO, (b) EDS image of Ni, (c) EDS image of Mn, (d) plan-view TEM image of LSMO-NiO on STO, (e) TEM image of a NiO nanopillar, and (f) schematic figure of the LSMO:NiO VAN structure grown on STO.

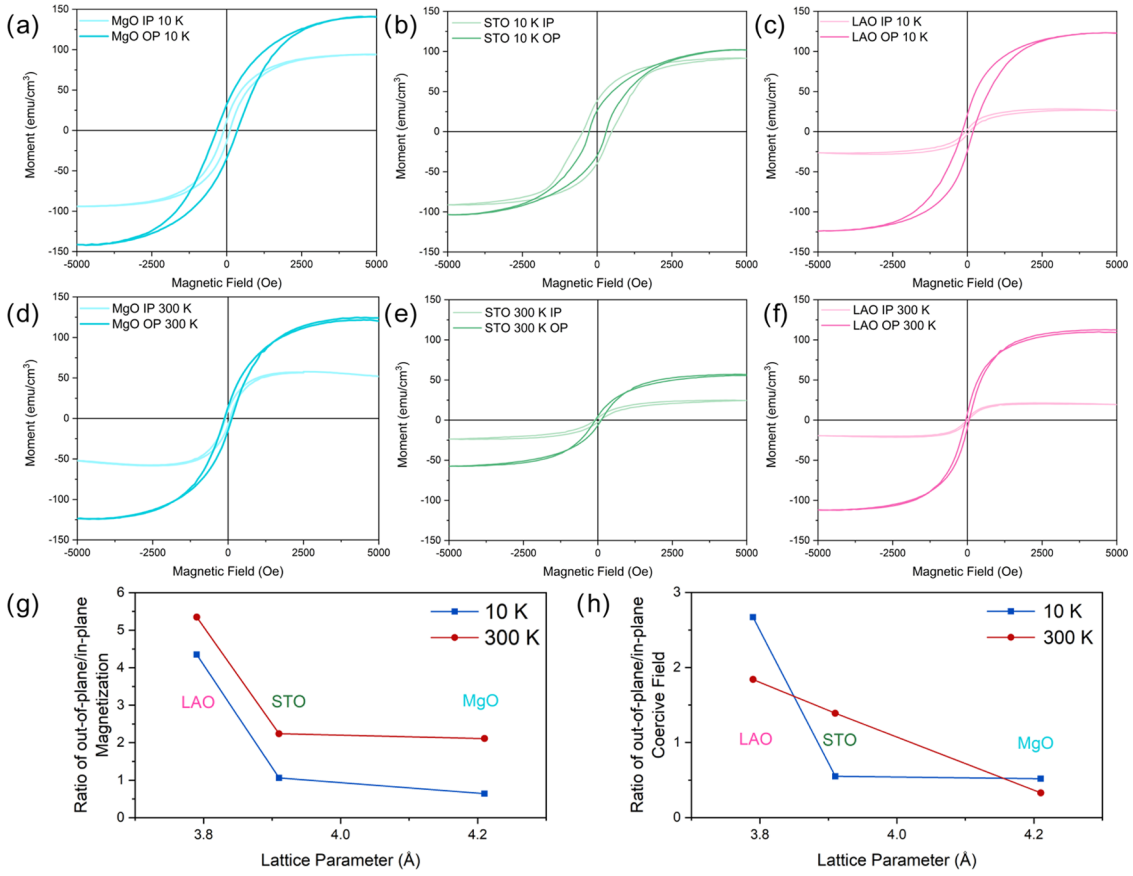

Figure 4. (a–c) Magnetic hysteresis loops for all films measured in the in-plane and out-of-plane directions at 10 K for MgO, STO, and LAO substrate samples, respectively, (d–f) magnetic hysteresis loops for all films measured in the in-plane and out-of-plane directions at 300 K for MgO, STO, and LAO substrate samples, respectively, (g) ratio of out-of-plane to in-plane magnetization saturation as a function of the substrate lattice parameter, (h) and ratio of out-of-plane to in-plane coercive field as a function of the substrate lattice parameter.

are highlighted relative to the LSMO matrix and have an average height of 17.47 nm. Figure 3d,e highlights the NiO nanopillars in plan-view images of the sample, showing that the nanopillars have formed in the LSMO matrix with some minor variation in diameter. The average pillar diameter was found to be 5.15 nm. The average film thicknesses of the films grown on LAO, STO, and MgO are 18.4, 17.4, and 13.9 nm, respectively. The TEM images of the films grown on LAO and MgO are shown in Figure S1. Both films showed phase separation based on the XRD data and STEM/EDS image analysis. Based on

https://dx.doi.org/10.1021/acsomega.0c02923
ACS Omega 2020, 5, 23793−23798

the above XRD results, obvious peaks from NiO and LSMO are identified for the case of LAO, whereas the NiO (002) and MgO (002) peaks overlapped for the MgO sample. In the STEM/EDS data, it is clear that NiO segregates at the MgO interface and thus grows highly strained with the MgO substrate. That is consistent with the overlapped NiO (002) and MgO (002) peaks in XRD data. In the case of LAO, the peak separation between NiO and LSMO was evidenced in the XRD data with the STEM/EDS data suggesting very fine NiO pillars in the LSMO matrix. Neither of the two samples grows in a distinguished nanopillar-in-matrix form as that of the STO sample.

The magnetic properties of all films were measured to analyze the effect of nanopillars and phase separation on the overall magnetic properties in the thin films. The magnetic saturation of the film grown on MgO at 10 K is 140 and 90 emu/cm^3 for an applied magnetization in the in-plane and out-of-plane, respectively. The magnetic saturation of the film on MgO at 300 K for the out-of-plane direction is 120 emu/cm^3 and the in-plane direction 57 emu/cm^3. For the film grown on the STO substrate, the magnetic saturation at 10 K is 92 and 98 emu/cm^3 in the in-plane and out-of-plane directions, respectively. For the STO film at 300 K, the magnetic saturation is 25 and 56 emu/cm^3 in the in-plane and out-of-plane directions, respectively. The film grown on the LAO substrate has a magnetic saturation at 10 K of 28 and 122 emu/cm^3 for an applied magnetization in the in-plane and out-of-plane directions, respectively. The film grown on the LAO substrate has a magnetic saturation at 300 K of 20 and 107 emu/cm^3 in-plane and out-of-plane directions, respectively. A stronger magnetization is consistently observed in all three films at 10 K relative to the 300 K measurement. Figure 4g,h shows the comparison of the ratio of the out-of-plane to in-plane saturation magnetization, and the coercive field in-plane and out-of-plane as a function of the lattice parameters for LAO, STO, and MgO, respectively. Interestingly, there exists a high degree of magnetic anisotropy for all of the samples. The LAO and STO substrate samples show clear out-of-plane anisotropy under both 10 and 300 K, while the MgO sample shows an obvious out-of-plane anisotropy for 300 K and an in-plane anisotropy under 10 K. This is actually consistent with the above microstructural analysis results from STEM/EDS where a NiO/LSMO VAN structure has been observed in the LAO and STO cases, while the MgO sample shows a NiO/LSMO bilayer structure with NiO segregated near the film-substrate interface. The coercive field ratio between the out-of-plane and in-plane for all three samples also follows a similar trend as that of the saturation magnetization ratio and decreases with the increasing substrate lattice parameters, i.e., the LAO and STO samples show obvious out-of-plane anisotropy, while the MgO one shows in-plane anisotropy under 300 K. Along these curves, the hysteresis loops close slightly and reopens back up, hinting an interplay between multiple ferromagnetic orders in the films. Traditionally, NiO is reported as an antiferromagnetic material, but it has been reported at sub-10 nm, NiO nanoparticles present ferromagnetic behavior.[30] Since the NiO pillar diameter is around 5 nm, these pillars may present a ferromagnetic response, causing this unique behavior as demonstrated by the hysteresis loops. At 300 K, LSMO has shown to have a significant decrease in magnetic response when compared to low temperature, which causes the weakening of the magnetic behavior that is seen in both the in-plane and out-of-plane results. For the MgO and LAO samples, the in-plane hysteresis loops are different, which may be explained by the nanostructure of the NiO regions. For the MgO sample, NiO forms nanoclusters concentrated along the substrate interface, and for the LAO sample, NiO forms a continuous layer along the substrate interface, both of which can be seen in the supplemental STEM images. The continuous NiO layer will form an antiferromagnetic layer within the film, causing the obvious weakening in the in-plane direction. Although NiO is a weaker ferromagnetic material than LSMO, NiO is clustered horizontally on the MgO substrate, causing a greater weakening of the in-plane magnetization when compared to the out-of-plane, though not to the extent of the NiO layer on the LAO substrate. The VAN structure also caused a reduction in the magnetization of the material overall, which could be due to the antiferromagnetic NiO nanopillars resulting in an overall reduction of the magnetic properties compared to the films without distinct nanostructures.

CONCLUSIONS

The lattice mismatch-induced strain alters the nucleation and orientation of the two phases during the growth of VAN thin films. Using the LSMO:NiO VAN system as a model system, we have shown that the growth morphology, two-phase separation, orientation of the two phases, and film properties are greatly influenced by the underlying substrates. The LSMO phase grew on each substrate in the predicted cube-on-cube growth orientation. Placing LSMO under tensile strain and NiO under compressive strain reduced the overall in-plane lattice mismatch of the system and allowed for a VAN structure to nucleate and grow on STO. Growing a distinct VAN structure led to interesting magnetic interaction between ferromagnetic NiO and ferromagnetic LSMO that was not seen in the films without a distinguishable nanostructure (i.e., samples on MgO and LAO). This work demonstrates that the substrate strain is critical in predicting and controlling the growth morphology of VAN nanostructures, tuning the properties of nanocomposite thin-film materials, and influencing the coupling of materials functionalities.

EXPERIMENTAL SECTION

PLD with a KrF laser (Lambda Physik, λ = 248 nm) at 10 Hz was used to fabricate the nanocomposite thin-film samples. The laser energy and fluence was 420 mJ and 7 J/cm^2, respectively. The nanocomposite thin films were made with an LSMO:NiO target (3:1 molar ratio) and grown on single-crystal STO (001), LAO (001), and MgO (001) substrates in 200 mTorr oxygen at 750 °C. After deposition, the thin films were cooled in 200 Torr oxygen at 5 °C/min. XRD (PANalytical Empyrean diffractometer) was used to determine the phases present. TEM (FEI Talos 200X) was used to determine the microstructure of the films with EDS mapping and high-resolution STEM. TEM samples were made with the standard manual grinding and dimpling process, followed by ion milling (PIPS II Gatan). Magnetic property measurements for in-plane and out-of-plane were done with a Magnetic Property Measurement System (MPMS) (MPMS Model 3, Quantum Design).

https://dx.doi.org/10.1021/acsomega.0c02923
ACS Omega 2020, 5, 23793−23798

■ ASSOCIATED CONTENT

Supporting Information

The Supporting Information is available free of charge at https://pubs.acs.org/doi/10.1021/acsomega.0c02923.

TEM and EDS data for the films grown on MgO and LAO substrates (PDF)

■ AUTHOR INFORMATION

Corresponding Author

Haiyan Wang − *School of Materials Engineering and School of Electrical and Computer Engineering, Purdue University, West Lafayette, Indiana 47907, United States;* orcid.org/0000-0002-7397-1209; Email: hwang00@purdue.edu

Authors

Bethany X. Rutherford − *School of Materials Engineering, Purdue University, West Lafayette, Indiana 47907, United States;* orcid.org/0000-0003-4149-9891

Bruce Zhang − *School of Electrical and Computer Engineering, Purdue University, West Lafayette, Indiana 47907, United States*

Xuejing Wang − *School of Materials Engineering, Purdue University, West Lafayette, Indiana 47907, United States*

Xing Sun − *School of Materials Engineering, Purdue University, West Lafayette, Indiana 47907, United States*

Zhimin Qi − *School of Materials Engineering, Purdue University, West Lafayette, Indiana 47907, United States*

Han Wang − *School of Materials Engineering, Purdue University, West Lafayette, Indiana 47907, United States;* orcid.org/0000-0002-6137-4802

Complete contact information is available at: https://pubs.acs.org/10.1021/acsomega.0c02923

Notes

The authors declare no competing financial interest.

■ ACKNOWLEDGMENTS

This work was supported by the U.S. National Science Foundation (NSF) (DMR-1565822 and DMR-2016453). B.X.R. acknowledges the support from the Purdue Doctoral Fellowship.

■ REFERENCES

(1) Huang, J.; Macmanus-driscoll, J. L.; Wang, H. New Epitaxy Paradigm in Epitaxial Self-Assembled Oxide Vertically Aligned Nanocomposite Thin Films. *J. Mater. Res.* **2017**, *32*, 4054−4066.

(2) Zhang, B.; Fan, M.; Li, L.; Jian, J.; Huang, J.; Wang, H.; Kalaswad, M.; Wang, H. Tunable Magnetic Anisotropy of Self-Assembled Fe Nanostructures within a La0.5Sr0.5FeO3 Matrix. *Appl. Phys. Lett.* **2018**, *112*, No. 013104.

(3) Fan, M.; Zhang, B.; Wang, H.; Jian, J.; Sun, X.; Huang, J.; Li, L.; Zhang, X.; Wang, H. Self-Organized Epitaxial Vertically Aligned Nanocomposites with Long-Range Ordering Enabled by Substrate Nanotemplating. *Adv. Mater.* **2017**, *29*, No. 1606861.

(4) Huang, J.; Tsai, C.-F.; Chen, L.; Jian, J.; Khatkhatay, F.; Yu, K.; Wang, H. Magnetic Properties of (CoFe2O4)x:(CeO2)1−x Vertically Aligned Nanocomposites and Their Pinning Properties in YBa2-Cu3O7−δ Thin Films. *J. Appl. Phys.* **2014**, *115*, No. 123902.

(5) Zhang, W.; Li, L.; Lu, P.; Fan, M.; Su, Q.; Khatkhatay, F.; Chen, A.; Jia, Q.; Zhang, X.; Macmanus-driscoll, J. L.; Wang, H. Perpendicular Exchange Biase Magnetotransport at the Vertical Heterointerfaces in La0.7Sr0.3MnO3:NiO Nanocomposites. *Appl. Mater. Interfaces* **2015**, *7*, 21646−21651.

(6) Wang, H.; Khatkhatay, F.; Jian, J.; Huang, J.; Fan, M.; Wang, H. Strain Tuning of Ferroelectric and Optical Properties of Rhombohedral-like BiFeO3 Thin Films on SrRuO3-Buffered Substrates. *Mater. Res. Bull.* **2019**, *110*, 120−125.

(7) Comes, R.; Liu, H.; Khokhlov, M.; Kasica, R.; Lu, J.; Wolf, S. A. Directed Self-Assembly of Epitaxial CoFe2O4−BiFeO3 Multiferroic Nanocomposites. *Nanoletters* **2012**, *12*, 2367−2373.

(8) Guzman, R.; Gazquez, J.; Rouco, V.; Palau, A.; Magen, C.; Varlea, M.; Arboil, J.; Obradors, X.; Puig, T. Strain-Driven Broken Twin Boundary Coherence in YBa2Cu3O7−δ Nanocomposite Thin Films. *Appl. Phys. Lett.* **2013**, *102*, No. 081906.

(9) Gutiérrez, J.; Llordes, A.; Gazquez, J.; Gibert, M.; Roma, N.; Ricart, S.; Pomar, A.; Sandiumenge, F.; Mestres, N.; Puig, T.; Obradors, X. Strong Isotropic Flux Pinning in Solution-Derived YBa2Cu3O7-x Nanocomposite Superconductor Films. *Nat. Mater.* **2007**, *6*, 367−373.

(10) Koep, E.; Jin, C.; Haluska, M.; Das, R.; Narayan, R.; Sandhage, K.; Snyder, R.; Liu, M. Microstructure and Electrochemical Properties of Cathode Materials for SOFCs Prepared via Pulsed Laser Deposition. *J. Power Sources* **2006**, *161*, 250−255.

(11) Kim, D. H.; Aimon, N. M.; Sun, X.; Ross, C. A. Compositionally Modulated Magnetic Epitaxial Spinel/Perovskite Nanocomposite Thin Films. *Adv. Funct. Mater.* **2014**, *24*, 2334−2342.

(12) He, H.-C.; Wang, J.-P.; Zhou, J.; Nan, C.-W. Ferroelectric and Ferromagnetic Behavior of Pb(Zr0.52Ti0.48)O3−Co0.9Zn0.1Fe2O4 Multilayered Thin Films Prepared via Solution Processing. *Adv. Funct. Mater.* **2007**, *17*, 1333−1338.

(13) Zhang, Z.; Zhang, L.; Hedhili, M. N.; Zhang, H.; Wang, P. Plasmonic Gold Nanocrystals Coupled with Photonic Crystal Seamlessly on TiO2 Nanotube Photoelectrodes for Efficient Visible Light Photoelectrochemical Water Splitting. *Nanoletters* **2013**, *13*, 14−20.

(14) Tsai, C.; Huang, J.; Lee, J.; Khatkhatay, F.; Chen, L.; Chen, A.; Su, Q.; Wang, H. Tunable Flux Pinning Landscapes Achieved by Functional Ferromagnetic Fe2O3:CeO2 Vertically Aligned Nanocomposites in YBa2Cu3O7 Thin Films. *Phys. C* **2015**, *510*, 13−20.

(15) Macmanus-Driscoll, J. L. Self-Assembled Heteroepitaxial Oxide Nanocomposite Thin Film Structures: Designing Interface-Induced Functionality in Electronic Materials. *Adv. Funct. Mater.* **2010**, *20*, 2035−2045.

(16) Zhang, W.; Ramesh, R.; Macmanus-driscoll, J. L.; Wang, H. Multifunctional, Self-Assembled Oxide Nanocomposite Thin Films and Devices. *MRS Bull.* **2016**, *40*, 736−745.

(17) Zhang, C.; Kim, D. H.; Huang, X.; Sun, X. Y.; Aimon, N. M.; Chua, S. J.; Ross, C. A. Magnetic and Photoluminescent Coupling in SrTi0.87Fe0.13O3−δ/ZnO Vertical Nanocomposite Films. *Appl. Mater. Interfaces* **2017**, *9*, 32359−32368.

(18) Tan, G.; Nakagawara, O.; Hattori, A. N.; Tanaka, H. Arrangement of Self-Assembled ZnO-NiO Nanostructures Using Topographical Templates towards Oxide Directed Self- Assembly. *AIP Adv.* **2018**, *8*, No. 115029.

(19) Macmanus-Driscoll, J. L.; Suwardi, A.; Wang, H. Composite Epitaxial Thin Films: A New Platform for Tuning, Probing, and Exploiting Mesoscale Oxides. *MRS Bull.* **2015**, *40*, 933−942.

(20) Chen, A.; Bi, Z.; Jia, Q.; Macmanus-driscoll, J. L.; Wang, H. Microstructure, Vertical Strain Control and Tunable Functionalities in Self-Assembled, Vertically Aligned Nanocomposite Thin Films. *Acta Mater.* **2013**, *61*, 2783−2792.

(21) Chen, A.; Hu, J.; Lu, P.; Yang, T.; Zhang, W.; Li, L.; Ahmed, T.; Enriquez, E.; Weigand, M.; Su, Q.; Wang, H.; Zhu, J.; Macmanus-driscoll, J. L.; Chen, L.; Yarotski, D.; Jia, Q. Role of Scaffold Network in Controlling Strain and Functionalities of Nanocomposite Films. *Sci. Adv.* **2016**, *2*, No. e1600245.

(22) Zhang, W.; Chen, A.; Bi, Z.; Jia, Q.; Macmanus-driscoll, J. L.; Wang, H. Interfacial Coupling in Heteroepitaxial Vertically Aligned Nanocomposite Thin Films: From Lateral to Vertical Control. *Curr. Opin. Solid State Mater. Sci.* **2014**, *18*, 6−18.

(23) MacManus-Driscoll, J. L.; Zerrer, P.; Wang, H.; Yang, H. A. O.; Yoon, J.; Fouchet, A.; Yu, R.; Blamire, M. G.; Jia, Q. Strain Control

and Spontaneous Phase Ordering in Vertical Nanocomposite Heteroepitaxial Thin Films. *Nat. Mater.* **2008**, *7*, 314−320.
(24) Zhu, Y. M.; Do, T. H.; Tra, V. T.; Yu, R.; Chu, Y.; Zhan, Q. Atomic Heterointerfaces and Electrical Transportation Properties in Self-Assembled LaNiO3−NiO Heteroepitaxy. *Adv. Mater. Interfaces* **2018**, *5*, No. 1701202.
(25) Chen, A.; Su, Q.; Han, H.; Enriquez, E.; Jia, Q. Metal Oxide Nanocomposites: A Perspective from Strain, Defect, and Interface. *Adv. Mater.* **2019**, *31*, No. 1803241.
(26) Su, Q.; Yoon, D.; Sisman, Z.; Khatkhatay, F.; Jia, Q.; Manthiram, A.; Wang, H. Vertically Aligned Nanocomposite La0.8Sr0.2MnO3-x/Zr0.92Y0.08O1.96 Thin Films as Electrode/Electrolyte Interfacial Layer for Solid Oxide Reversible Fuel Cells. *Int. J. Hydrogen Energy* **2013**, *38*, 16320−16327.
(27) Huang, J.; Wang, X.; Hogan, N. L.; Wu, S.; Lu, P.; Fan, Z.; Dai, Y.; Zeng, B.; Starko-bowes, R.; Jian, J.; Wang, H.; Li, L.; Prasankumar, R. P.; Yarotski, D.; Sheldon, M.; Chen, H.; Jacob, Z.; Zhang, X.; Wang, H. Nanoscale Artificial Plasmonic Lattice in Self-Assembled Vertically Aligned Nitride−Metal Hybrid Metamaterials. *Adv. Sci.* **2018**, *5*, No. 1800416.
(28) Wang, B.; You, L.; Ren, P.; Yin, X.; Peng, Y.; Xia, B.; Wang, L.; Yu, X.; Poh, S. M.; Yang, P.; Yuan, G.; Chen, L.; Rusydi, A.; Wang, J. Oxygen-Driven Anisotropic Transport in Ultra-Thin Manganite Films. *Nat. Commun.* **2013**, *4*, No. 2778.
(29) Sun, X.; Li, Q.; Huang, J.; Fan, M.; Rutherford, B. X.; Paldi, R. L.; Jian, J.; Zhang, X.; Wang, H. Strain-Driven Nanodumbbell Structure and Enhanced Physical Properties in Hybrid Vertically Aligned Nanocomposite Thin Films. *Appl. Mater. Today* **2019**, *16*, 204−212.
(30) Madhu, G.; Maniammal, K.; Biju, V. Defecr Induced Ferromagnetic Interaction in Nanostructured Nickel Oxide with Core-Shell Magnetic Structure: The Role of Ni2+ and O2- Vacancies. *Phys. Chem. Chem. Phys.* **2016**, *18*, 12135−12148.

https://dx.doi.org/10.1021/acsomega.0c02923
ACS Omega 2020, 5, 23793−23798